

## 생분해성 Poly(ethylene succinate-co-ethylene oxalate-co-diethylene glycol succinate): Ethylene Oxalate 양에 따른 Poly(ethylene succinate) 물성 연구

Chunyan Liu<sup>†</sup> 

Department of Chemical Engineering, Chengde Petroleum College  
(2020년 11월 4일 접수, 2021년 1월 4일 수정, 2021년 1월 12일 채택)

### Biodegradable Poly(ethylene succinate-co-ethylene oxalate-co-diethylene glycol succinate): Effects of a Small Amount of Ethylene Oxalate Content on the Properties of Poly(ethylene succinate)

Chunyan Liu<sup>†</sup> 

Department of Chemical Engineering, Chengde Petroleum College, Chengde 067000, Hebei, China  
(Received November 4, 2020; Revised January 4, 2021; Accepted January 12, 2021)

**Abstract:** In this work, poly(ethylene succinate-co-0.3 m% ethylene oxalate-co-0.6 m% diethylene glycol succinate) (PEED) and poly(ethylene succinate-co-0.6 m% diethylene glycol succinate) (PED) with a similar weight-average molar mass ( $M_w$ ) of about  $6 \times 10^4$  g/mol were synthesized by a two-step melt polycondensation method to investigate whether the strong-acting ethylene oxalate groups in the molecular chain of poly(ethylene succinate) (PES) could improve the crystallization rate and physical properties of PES. As a result, PEED crystallized faster under isothermal melt crystallization condition and the density of PEED spherulites also increased, indicating ethylene oxalate significantly acted as a nucleating agent. Relative to PED, PEED presented a similar tensile strength, yet its Young's modulus increased by 13%, and elongation at break increased by 72%, indicating that 0.3 m% of ethylene oxalate could improve the physical properties of PES. This study provides a new strategy for improving the crystallization rate of PES.


**Keywords:** poly(ethylene succinate), ethylene oxalate, diethylene glycol succinate, crystallization rate, mechanical property.

## Introduction

Poly(ethylene succinate) (PES) has received enormous interest due to the advantage of biocompatibility, biodegradability, good processability, relatively high melting temperature, and thermal stability.<sup>1-3</sup> It is a semi-crystalline polymer with a low glass transition temperature ( $T_g$ ), resulting in its good processability and physical properties, as well as degradation behaviors, which are highly dependent on its crystallization behaviors.<sup>10</sup> Only after the completion of crystallization, PES can be shaped. PES with improved physical properties can be applied to the field of film and spinning. However, its relatively poor mechanical properties and slow crystallization rate have limited the wider application of PES.

The properties of PES can be regulated by compounding with nanofillers and co-polymerization with components or polymers.<sup>3-16</sup> PES based nanocomposites, such as PES/ POSS (polyhedral oligomeric silsesquioxanes), PES/reduced graphene, PES/SiO<sub>2</sub>, and PES/f-MWNTs (multi-walled carbon nanotubes),<sup>4-6,8</sup> are usually helpful to both accelerate the crystallization process and improve the physical properties. For example, Teng *et al.*<sup>4</sup> reported that both the crystallization rate and storage modulus of PES/Tsib-POSS nanocomposites were remarkably enhanced, relative to those of neat PES.

On the contrary, PES-based biodegradable copolyesters usually hold reduced crystallization rate compared with PES due to the increased disturbance of molecular chains, such as poly(ethylene succinate-co-butylene succinate), poly(ethylene succinate-co-ethylene suberate), poly(ethylene succinate-co-diethylene glycol succinate), poly(ethylene succinate-co-octamethylene succinate), and poly[propylene-co-(ethylene succinate)].<sup>9,11-14</sup> Qiu<sup>9</sup> reported that the crystallization rates,

<sup>†</sup>To whom correspondence should be addressed.  
chunyanliu2006@163.com, 0000-0002-6920-0110  
©2021 The Polymer Society of Korea. All rights reserved.

melting temperature ( $T_m$ ) and spherulitic growth rates of poly(ethylene succinate-*co*-ethylene suberate) copolyesters with increasing the ESub composition were decreased.

There are a few reports of increasing the crystallization rate of PES by chain extender copolymerization.<sup>10,15</sup> Zeng *et al.* has reported that the crystallization rate of PES segments of poly(ethylene succinate)-*b*-poly(butylene succinate) (PES-*b*-PBS) multi-block copolymers can be accelerated by the crystals of PBS regarded as the heterogeneous nucleating agents since that PBS segments will first crystallize in the cooling process of the melts.<sup>15</sup> In addition, Zeng *et al.* has also reported the random copolymer, a segmented poly(ester urethane) ionomer (PESI) consisting of soft and hard segments, can be also dramatically accelerated the crystallization rate of PES due to the aggregation of hard segments induced by the ionic interactions.<sup>10</sup>

However, there is not co-polyester obtained by a two-step melt polycondensation method using a small molecule as the third monomer showing the improvement of the crystallization rate and physical properties. As mentioned above, it is possible to accelerate the crystallization rate of PES by introducing powerful monomers into PES molecular chain.

According to the previous work, polyethylene oxalate (PEOX) and diethylene oxalate (EOX) have a high melting point due to their high polarity.<sup>20,21</sup> Moreover, polyoxalates are readily synthesized from bio-renewable resources, a significant sustainability advantage over fossil fuel-based polymers.<sup>17,18</sup> Therefore, the PES co-polyester containing high polarity EOX units should theoretically show the enhanced crystallization rate and physical properties relative to neat PES.

In this study, poly(ethylene succinate-*co*-0.3 m% ethylene oxalate-*co*-0.6 m% diethylene glycol succinate) (PEED) and poly(ethylene succinate-*co*-0.6 m% diethylene glycol succinate) (PED) with a similar weight-average molar mass of about  $6 \times 10^4$  g/mol were synthesized by a two-step melt polycondensation method. Thus, the effect of a small amount of EOX content on the properties of PES was investigated in detail.

## Experimental

**Materials.** Ethylene glycol was purchased from Shanghai Aladdin BioChem Technology Co., Ltd.; Shanghai, China. Triphenyl phosphate (TPP) and succinic acid were purchased from Shanghai Macklin BioChem Technology Co., Ltd.

Shanghai, China. Oxalic acid ( $\text{H}_2\text{C}_2\text{O}_4 \cdot 2\text{H}_2\text{O}$ ), zinc acetate ( $\text{ZnAc}_2$ ), and antimony trioxide ( $\text{Sb}_2\text{O}_3$ ) were purchased from Tianjin Chemical Reagent Plant III Factory, Tianjin, China.

**Preparation of Copolymers.** To a three-necked flask equipped with a mechanical stirrer, ethylene glycol (10.6 g, 0.171 mol), succinic acid (15 g, 0.127 mol) were added.  $\text{ZnAc}_2$  (0.045 g) and  $\text{Sb}_2\text{O}_3$  (0.015 g) were used as the catalyst and 0.03 g of TPP was used as the antioxidant. 0 g and 3.20 g oxalic acid were added for PED and PEED, respectively. The mixture was placed one week at room temperature and then heated to 180 °C with a 20 mL min<sup>-1</sup> nitrogen flow. The polycondensation was completed until no water was produced (about 3 h). The mixture was then heated to 220-230 °C under the pressure of 100 Pa. After 4-6 h, the synthesis procedure was finished when the stirring speed of the stirring paddle slowed down sharply. The system was cooled to room temperature. The obtained products were dissolved in chloroform and precipitated by methanol for several times before they were further dried under vacuum at 50 °C for 72 h to remove any residual solvent. The products were obtained as white solid for PED and light yellow solid for PEED.

**Characterizations.** Nuclear magnetic resonance (<sup>1</sup>H NMR) spectra were recorded by a Bruker (USA) AVIII 600 MHz NMR spectrometer using  $\text{CDCl}_3$  as the solvent and TMS as the internal standard. The weight-average molecular weight ( $M_w$ ) and polydispersity index (PDI) of PES samples were measured on a Waters (USA) gel permeation chromatography (GPC) instrument using dimethylformamide (DMF) as the solvent at room temperature. Differential scanning calorimetry (DSC) measurements were performed on a Perkin Elmer (USA) Diamond DSC instrument. The dried samples were heated to 130 °C at a heating rate of 60 °C/min under nitrogen atmosphere, held for 3 min, then cooled to -30 °C at a rate of 60 °C/min, held for 3 min, and then heated again to 130 °C at a rate of 10 °C/min, and finally cooled to -30 °C at a rate of 10 °C/min; the second melting and cooling processes were recorded. For the isothermal crystallization procedure, the samples were cooled to the predetermined crystallization temperature ( $T_c$ ) at 60 °C/min after any previous thermal history was erased and crystallized isothermally for a considerable time to ensure complete crystallization. An Olympus BX-51 polarized optical microscopy with a digital camera was used for the observation of the crystallization process. The samples were heated and pressed by sandwiching a tiny pellet of the sample between two glass slides with a film thickness of about 100 μm, com-

pressing at 140 °C for 5 min, and then cooled and annealed at 70 °C for 1 h before capturing the photographs. The mechanical properties of the copolymers were tested at room temperature with an MTS (USA) E44.304 universal testing machine at a speed of 50 mm/min. The dumbbell-shaped samples were obtained by injection molding from 140 to 40 °C with a size of 25×5×2 mm<sup>3</sup>. Three parallel specimens were tested for each polyester and the values were averaged. Wide-angle X-ray diffraction (WAXD) experiments were performed by a Bruker (USA) D8 advance X-ray diffractometer at room temperature at 2°/min. The thermal stability properties of different copolyesters were studied by the thermogravimetric analyzer (TGA) (Pyris 6, Perkin Elmer Co., USA) in the following manner: the sample was heated at a rate of 20 °C/min from 30 to 700 °C under a nitrogen atmosphere, and the degradation process was recorded. The temperature data at different weight loss were taken from the curves.

## Results and Discussion

**Chemical Structure and Molecular Weights of the Copolymers PED and PEED.** <sup>1</sup>H NMR spectra can be used to accurately detect the chemical composition of products. Figure 1 showed the <sup>1</sup>H NMR spectra of both samples and the signals had been assigned to the corresponding protons. The signals located at 4.30 and 2.67 ppm were ascribed to the protons of the ethoxyl (H3) and the succinyl groups (H4), respectively. The proton (H6) signals of the terminal methylene groups are located at 3.82 ppm.

It was noted that the signals of the glycol oxalate ester were detectable from protons (H1 and H2) in glycol residues on the <sup>1</sup>H NMR spectra of PEED, while there was almost no absorbance of protons at the same chemical shift on the <sup>1</sup>H NMR spectra of PED. In addition, two triplet signals appeared at 4.25 and 3.70 ppm, which were assigned to the protons of the two methylene at the diethylene glycol succinate (DEOS) groups.<sup>13,22</sup> They were produced by the dehydration side reaction between ethylene glycols.

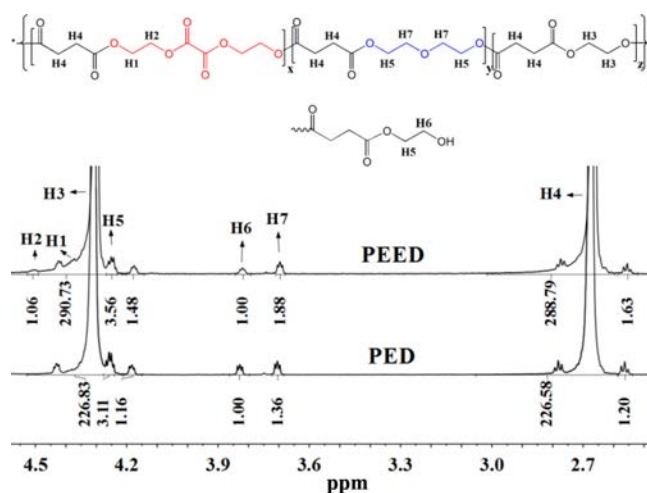


**Figure 1.** <sup>1</sup>H NMR spectra of PEED and PED.

By using eqs. (1) and (2), the molar content of EOX and DEOS units in the resulted polyesters could be calculated, respectively.

$$EOX\% = \frac{I_{H1}}{I_{H1} + I_{H4}} \quad (1)$$

$$DEOS\% = \frac{I_{H7}}{I_{H1} + I_{H4}} \quad (2)$$

The <sup>1</sup>H NMR spectra revealed that the molar percentage content of the DEOS unit in both PED and PEED was about 0.6%, and the molar percentage content of the EOX unit in PEED was about 0.3%.

It is worth noting that the utilization rate of oxalic acid is very low. The main reason is that oxalic acid has a low boiling point and sublimates at 150-160 °C while the esterification temperature is 180 °C in this study. Moreover, the hydrolyzability of oxalate makes its utilization rate very low in direct-condensation polymerization.<sup>18-21</sup>

The degrees of polymerization and number average molecular weight ( $M_n$ ) were calculated from the integrations of the ethoxyl protons and the terminal methylene protons (Table 1).

**Table 1. Chemical Composition and Molecular Weights for PED and PEED**

Samples	Components <sup>a</sup>		$n^b$	$M_n^c$ (g/mol)/10 <sup>4</sup>	$M_w^d$ (g/mol)/10 <sup>4</sup>	$M_n^d$ (g/mol)/10 <sup>4</sup>	PDI <sup>d</sup>
	DEOS (%)	EOX (%)					
PED	0.6	/	226	3.2	6.3	4.2	1.5
PEED	0.6	0.3	289	4.2	6.0	4.3	1.4

<sup>a</sup>Contents of DEOS and EOX were calculated by <sup>1</sup>H NMR. <sup>b</sup>Degrees of polymerization were calculated by <sup>1</sup>H NMR. <sup>c</sup>Molecular weights were calculated by <sup>1</sup>H NMR. <sup>d</sup>Molecular weights and polydispersity index were measured by GPC (Figure 2).

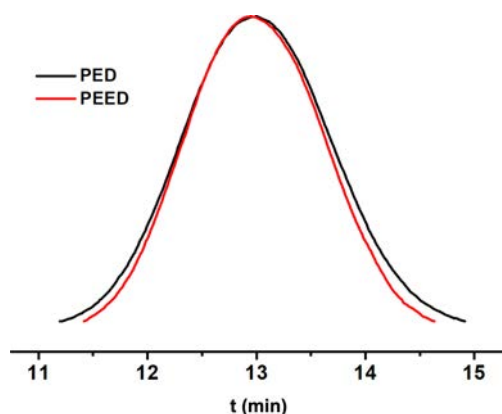


Figure 2. GPC spectra of PEED and PED polyesters.

Meanwhile, molecular weights and polydispersity index of both PED and PEED were measured by GPC using DMF as the solvent (Figure 2). Perfectly, the number-average molecular weight obtained by the two methods was very similar.

Figure 3(A) is the FTIR spectra of PEOX, PEED, and PED polyesters. In Figure 3(A), the characteristic absorption peaks were attributed to the stretching vibration of -OH, -CH<sub>2</sub>, O=C, and C-O-C groups are observed at 3200~3800, 2500~3200, 1560~2300, and 1300~1100 cm<sup>-1</sup>, respectively. As can be seen in Figure 3(A), there was no remarkable difference in the FTIR spectra of PEED and PED polyesters, due to a minor amount of EOX unit. Yet, the enhancement of hydrogen bonding between -C=O and -OH was observed, as can be seen from the comparison of FTIR spectra of PEED and PED at 1600~1900 cm<sup>-1</sup> (Figure 3(B)) and 3200~3700 cm<sup>-1</sup> (Figure 3(C)), respectively. The slight increment of hydrogen bonding between C=O and OH groups suggested that the group O=C-C=O, due to its strong polarity, was easier to form a hydrogen bond with the hydroxyl group.

In a word, PEED and PED with similar  $M_w$  and PDI were synthesized successfully. The effect of the small amount of EOX with strong interactions on the properties of PES was capable of being studied accurately because the chemical structure of PED and PEED differs only in 0.3 m% EOX component. Therefore, their thermal properties, crystallization kinetics, spherulitic morphology, and mechanical properties were investigated in detail as below.

**DSC Analysis of PED and PEED Samples.** Figure 4 showed the DSC heating and cooling scans of PED and PEED samples. Table 2 summarized the DSC data. On the heating scans (Figure 4(A)), the glass transition temperature ( $T_g$ ), the cold crystallization temperature ( $T_{cc}$ ), and the melting temperature ( $T_m$ ) of PED and PEED samples presented almost the

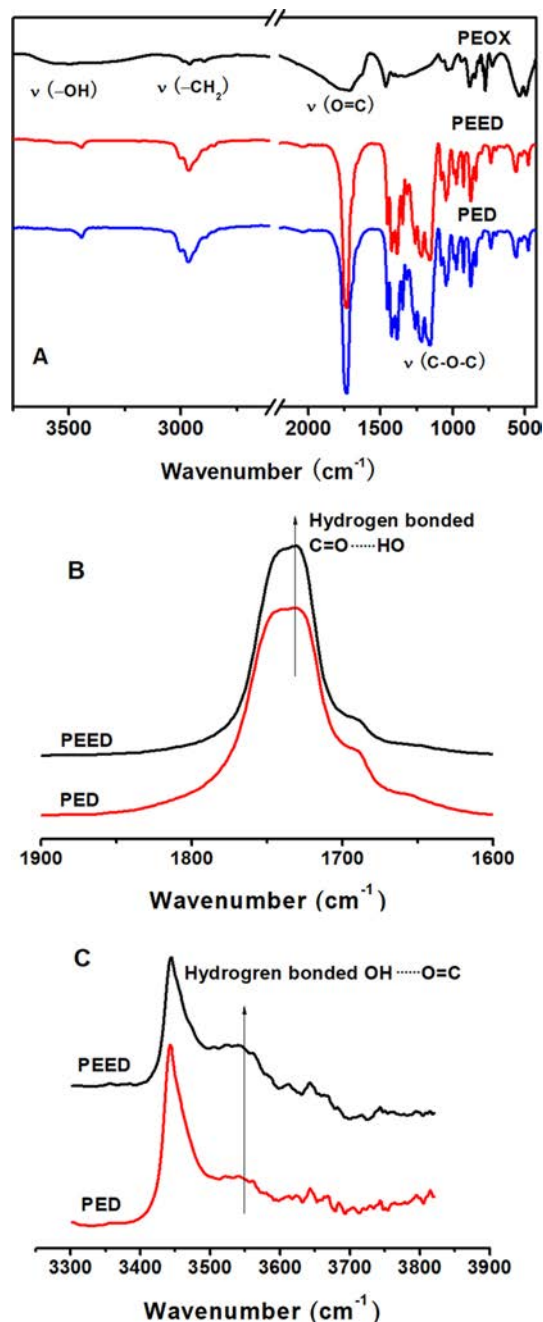
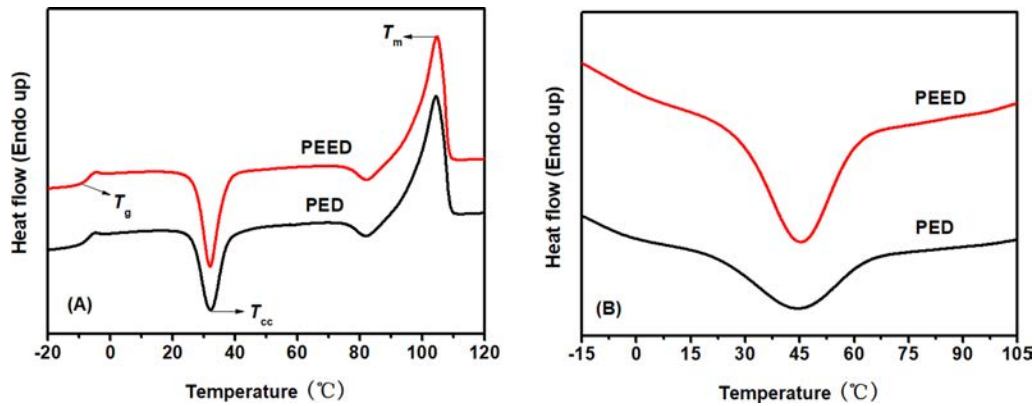


Figure 3. FTIR spectra of PEOX, PEED and PED polyesters (A) and comparison of FTIR spectra of PEED and PED at 1600~1900 cm<sup>-1</sup> (B); 3200~3800 cm<sup>-1</sup> (C).

same value, respectively, indicating that a small amount of EOX component incorporated had little influenced on melting behavior of PES copolymer. For melting enthalpy ( $\Delta H_m$ ) and cold crystallization enthalpy ( $\Delta H_{cc}$ ), both those values of PEED were larger than those values of PED, indicating that PEED showed a larger crystallinity and higher crystallization



**Figure 4.** DSC heating scans (A); cooling scans (B) of PED and PEED samples at a scan rate of 10 °C/min.

**Table 2. Thermal Parameters of PED and PEED Samples**

Samples	$T_g$ (°C)	$T_{cc}$ (°C)	$\Delta H_{cc}$ (J·g <sup>-1</sup> )	$T_m$ (°C)	$\Delta H_m$ (J·g <sup>-1</sup> )	$T_c$ (°C)	$\Delta H_c$ (J·g <sup>-1</sup> )	$X_c^a$
PED	-8.3	32.1	27.0	105	60.8	44.4	27.3	33
PEED	-8.2	32.1	37.1	105	68.4	45.6	40.4	39

<sup>a</sup>Calculated by XRD data.

ability. The results of the WAXD calculation also proved this observation ( $X_c$  in Table 2 and XRD curves in Figure 7). It was worth noting that both PED and PEED presented a higher  $T_m$  of about 105 °C due to only 0.6 m% of the DEOS unit existing in their chemical structure. The previous work had shown that PES with more DEOS content displayed lower  $T_m$  below 100 °C.<sup>13</sup> On the cooling scans (Figure 4(B)), a relative broad crystallization peak could be observed at 44.4 °C for PED of which  $\Delta H_c$  was 27.3 J·g<sup>-1</sup>; however, the  $T_c$  and  $\Delta H_c$  of PEED with a narrow and high crystallization peak increased to 45.6 °C and 40.4 J·g<sup>-1</sup>, respectively. As a result, compared with PED, PEED displayed a better crystallization ability. In brief, 0.3 m% of the EOX component incorporated into the PES polymer could enhance the crystallization ability of PES but had little influence on other DSC melting behaviors.

**Isothermal Crystallization Kinetics.** The crystallization behaviors of PED and PEED were further studied by DSC under the isothermal melt-crystallization conditions at various crystallization temperature ( $T_c$ ) after erasing any previous thermal history. Figure 5 displayed the development of relative crystallinity ( $X_t$ ) with crystallization time ( $t$ ) for two samples, showing the typical S-shaped features. For PED and PEED, increasing  $T_c$  resulted in longer crystallization time, indicating a slower crystallization rate. Furthermore, the time needed to finish crystallization for PED at various  $T_c$  was longer than those of PEED, indicating that the EOX unit could enhance the

crystallization rate of PES segments, which should be ascribed to the formation of the aggregates of EOX unit as well as EOX unit and others due to the high polarity of EOX unit. These aggregates could induce the crystallization of PES segments, which should be similar to the explanation of the previous work reported by Zeng *et al.*<sup>10</sup>

The above-acquired data of  $X_t$  and  $t$  were further analyzed by the Avrami equation to investigate the isothermal crystallization kinetics. The equation assumes that the relative crystallinity develops with crystallization time  $t$  as

$$1 - X_t = \exp(-kt^n) \quad (1)$$

where  $k$  is a rate constant depending on nucleation and crystalline growth rate, and  $n$  is the Avrami exponent which denotes the nature of the nucleation and growth process.<sup>23</sup>

The Avrami plots of PED and PEED samples at various  $T_c$  were shown in Figure 6. The almost parallel straight lines were observed for both samples at various  $T_c$ , suggesting that the Avrami equation could describe the isothermal crystallization kinetics of the two samples. The  $k$  and  $n$  values were calculated from the intercepts and slopes of the lines, respectively, which were listed in Table 3. The  $n$  values for PED and PEED were ranging from 2.7 to 3.1, indicating the same crystallization mechanism of the copolymers and may correspond to a three-dimensional spherulitic growth with a thermal nucleation.<sup>24</sup>

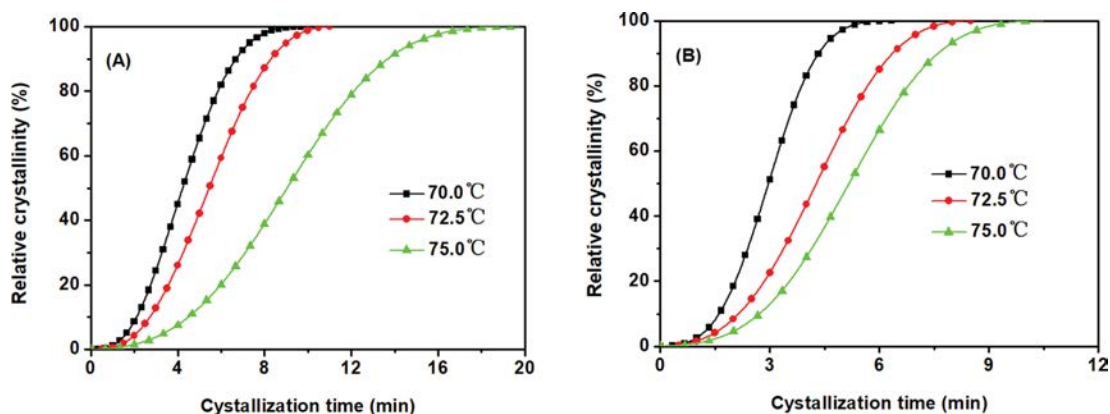


Figure 5. Development of relative crystallinity with crystallization time, (A) PED; (B) PEED.

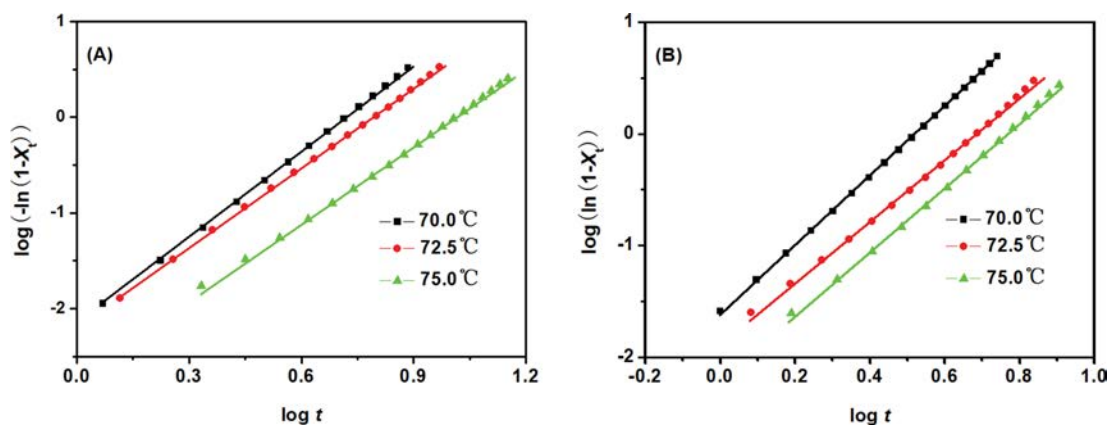


Figure 6. The related Avrami plots for (A) PED; (B) PEED.

Taking the unit of  $k$  ( $\text{min}^{-n}$ ) and the different  $n$  values into account, the crystallization half-time ( $t_{0.5}$ ) values presenting the time for the samples to approach half of the final crystallinity were calculated by the following equation to compare the crystallization rates of PED and PEED. Table 3 listed  $t_{0.5}$  values of PED and PEED at various  $T_c$ . For both samples, a higher  $T_c$  led to a greater  $t_{0.5}$ , indicating a slower crystallization rate. Furthermore, relative to PED, a shorter  $t_{0.5}$  for PEED was obtained at the same  $T_c$ , suggesting that PEED had a faster crystallization rate.

$$t_{0.5} = \left( \frac{\ln 2}{k} \right)^{1/n} \quad (2)$$

At the same time,  $t_{0.5}$  of PEED at 70 °C is only 3 min which is close to the value of 2.6 min of PESI3 reported by Zeng and nearly half of the value of 5.8 min of PES/oib-POSS reported by Teng, indicating PEED holds a very fast crystallization rate.<sup>4,10</sup>

**Spherulitic Morphology of PED and PEED.** Spherulitic

Table 3. Parameters of PED and PEED at Different  $T_c$

Samples	$T_c$	$n$	$k$ ( $\text{min}^{-n}$ )	$t_{0.5}$ (min)
PED	75.0 °C	2.7	$1.91 \times 10^{-3}$	8.9
	72.5 °C	2.8	$6.31 \times 10^{-3}$	5.4
	70.0 °C	3.0	$6.61 \times 10^{-3}$	4.7
PEED	75.0 °C	2.9	$5.75 \times 10^{-3}$	5.2
	72.5 °C	2.8	$1.26 \times 10^{-2}$	4.2
	70.0 °C	3.1	$2.40 \times 10^{-2}$	3.0

morphology and crystal structure of PED and PEED were also studied by POM and WAXD, respectively. Figure 7(b) and 7(c) showed the spherulitic morphology of the samples crystallized at 70 °C. The two samples both showed the typical Maltese cross extinction pattern. For PED, its spherulites were larger than those of PEED, which suggested that PEED had higher nucleation ability than PED. This higher nucleation ability of PEED was caused by the EOX unit enhancing the number of hydrogen bonding which acted as a nucleus and

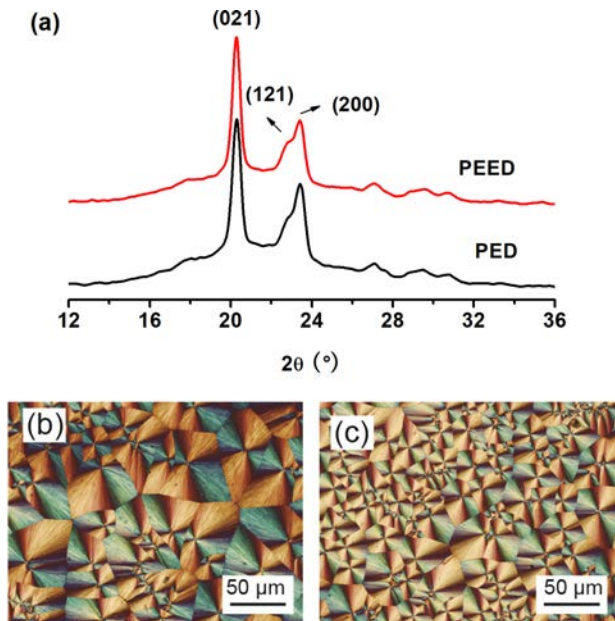


**Figure 7.** (a) WAXD profiles of PED and PEED; the spherulite morphologies of (b) PED; (c) PEED.

induced the crystallization of PES segments.

The WAXD patterns of both PES samples were displayed in Figure 7(a) after crystallizing at 80 °C for three days.<sup>16</sup> And their degrees of crystallinity ( $X_c$ ) were listed in Table 3. PED and PEED presented almost the same three main diffraction peaks at 20.1°, 20.4°, and 23.2°, which corresponded to (021), (121), and (200) of PES, respectively.<sup>9,13</sup> Therefore, both PED and PEED samples had the same crystal structures with PES, regardless of the EOX component. However, from Table 3, PED had a crystallinity of 33, while PEED had a crystallinity of 39, indicating that the EOX component could enhance the crystallinity of the PES copolymer.

To sum up, 0.3 m% of EOX component incorporated into the PES copolymer had no influence on the crystal structure and crystalline morphology of PES but increased the number of spherulites in the same field of vision and the crystallinity of the polymer.

**Mechanical Properties of the Copolymers.** Figure 8 displayed the stress-strain curves of the copolymers. Both sam-

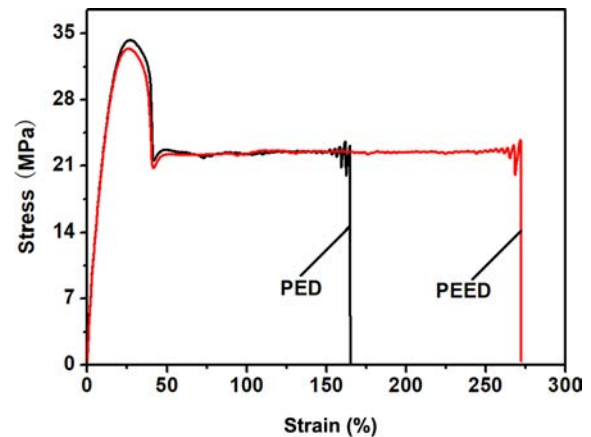


**Figure 8.** Stress-strain curves for PED and PEED.

ples showed a ductile fracture. Table 4 summarized the values of their mechanical properties. PED and PEED both showed almost the same yield elongation (about 33%) and yield strength (about 33.5 MPa), indicating that a minor amount of EOX unit displayed no remarkable influence on yield behavior of PES segments. Yet, PED gave a tensile strength of 33.9 MPa, Young's modulus of 305 MPa, elongation at break of 150% and 3880 MPa·m<sup>0.5</sup> of fracture energy; PEED presented a tensile strength of 33.3 MPa, Young's modulus of 340 MPa, elongation at break of 259% and 6235 MPa·m<sup>0.5</sup> for fracture energy. Compared with PED, PEED exhibited improved elongation at break, Young's modulus, and fracture energy due to its higher crystallinity but a smaller crystal size. However, tensile strength could be regarded as the same as that of PED.

**TGA Analysis.** Figure 9 showed the TGA curves for PED and PEED. According to Figure 9, the values of  $T_{2\%}$  (temperature of decomposition 2% of sample weight) for PED and PEED were 340 °C and 310 °C, respectively, indicating that both PED and PEED had a good thermal stability. However, the thermal stability of PEED was lower than that of PED due to the lower thermal stability of EOX units.<sup>20</sup>

## Conclusions

In this work, biodegradable P(ES-co-0.3m%EOX-co-0.6m%

**Table 4. Mechanical Properties of the Polymers**

Samples	$E$ (MPa)	$\sigma_y$ (MPa)	$\epsilon_x$ (%)	$\sigma_t$ (MPa)	$\epsilon_b$ (%)	$E_f$ (MPa·m <sup>0.5</sup> )
PED	305±5	33.9±0.3	33±3	33.9±0.3	150±15	3880
PEED	340±7	33.3±0.1	33±3	33.3±0.1	259±3	6235

$E$ : Young's modulus.  $\sigma_y$ : Yield strength;  $\sigma_t$ : Tensile strength.  $\epsilon_x$ : Yield elongation.  $\epsilon_b$ : Elongation at break.  $E_f$ : Fracture energy.

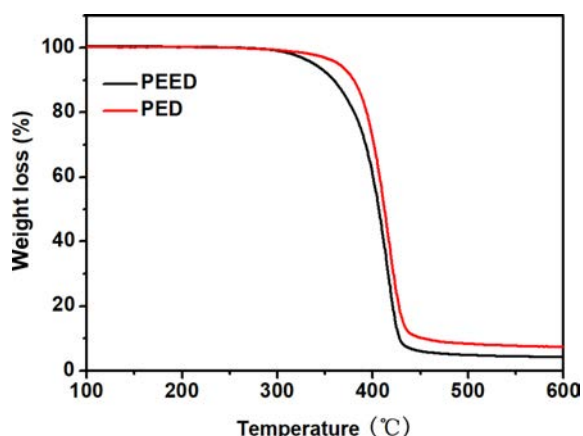


Figure 9. TGA curves for PED and PEED.

DEOS) (PEED) and P(ES-*co*-0.6m%DEOS) (PED) had been synthesized by a two-step melt polycondensation method. Both of them had a weight-average molar mass of about  $6 \times 10^4$  g/mol measured by GPC. The effect of the EOX unit on the properties of PES was studied in detail. Enhancement, due to the EOX unit strong polarity, of the number hydrogen bonding which acted as a nucleus, induced the higher nucleation ability of PEED. As a result, although the copolymer PEED had the same crystallization mechanisms as PED, it displayed a faster crystallization rate than that of PED. Moreover, PEED also had larger elongation at break, Young's modulus, and fracture energy than those of PED, due to much smaller spherulites size and more interactions of molecules. The thermal stability of PEED was slightly lower than that of PED due to the lower thermal stability of EOX units.

## References

1. Abdali, Z.; Logsetty, S.; Liu, S. Bacteria-Responsive Single and Core-Shell Nanofibrous Membranes Based on Polycaprolactone/ Poly(ethylene succinate) for On-Demand Release of Biocides. *ACS Omega* **2019**, *4*, 4063-4070.
2. Okur, N. U.; Filippousi, M.; Okur, M. E.; Ayla, S.; Caglar, E. S.; Yoltas, A.; Siafaka, P. I. A Novel Approach for Skin Infections: Controlled Release Topical Mats of Poly(Lactic Acid)/Poly (Ethylene Succinate) Blends Containing Voriconazole. *J. Drug. Deliv. Sci. Tec.* **2018**, *46*, 74-86.
3. Teng, S.; Qiu, Z. Enhanced Crystallization and Mechanical Properties of Biodegradable Poly(ethylene succinate) by Octaisobutyl-Polyhedral oligomeric silsesquioxanes in their nanocomposites. *Thermochim. Acta* **2017**, *649*, 22-30.
4. Teng, S. Q.; Jiang, Z. G.; Qiu, Z. B. Effect of Different POSS Structures on the Crystallization Behavior and Dynamic Mechanical Properties of Biodegradable Poly(Ethylene Succinate). *Polymer* **2018**, *163*, 68-73.
5. Vasileiou, A. A.; Papageorgiou, G. Z.; Kontopoulou, M.; Docoslis, A.; Bikiaris, D. Covalently Bonded Poly(Ethylene Succinate)/SiO<sub>2</sub> Nanocomposites Prepared by In Situ Polymerization. *Polymer* **2013**, *54*, 1018-1032.
6. Zhu, S. Y.; Zhao, Y. Y.; Qiu, Z. B. Crystallization Kinetics and Morphology Studies of Biodegradable Poly(Ethylene Succinate)/ multi-walled Carbon Nanotubes Nanocomposites. *Thermochim. Acta* **2011**, *517*, 74-80.
7. Asadi, V.; Jafar, S. H.; Khonakdar, H. A.; Häubler, L.; Wagenknecht, U. Poly(ethylene succinate) Nanocomposites Containing Inorganic WS<sub>2</sub> Nanotubes with Improved Thermal Properties: A Kinetic Study. *Composites Part B* **2016**, *98*, 496-507.
8. Jing, X. J.; Qiu, Z. B. Influence of Thermally Reduced Graphene Low-loadings on the Crystallization Behavior and Morphology of Biodegradable Poly(ethylene succinate). *Ind. Eng. Chem. Res.* **2014**, *53*, 498-504.
9. Qiu, S. T.; Su, Z. Q.; Qiu, Z. B. Crystallization Kinetics, Morphology, and Mechanical Properties of Novel Biodegradable Poly(ethylene succinate-*co*-ethylene suberate) Copolyesters. *Ind. Eng. Chem. Res.* **2016**, *55*, 10286-10293.
10. Zeng, J. B.; Wu, F.; Huang, C. L.; He, Y. S.; Wang, Y. Z. Urethane Ionic Groups Induced Rapid Crystallization of Biodegradable Poly(ethylene succinate). *ACS Macro Lett.* **2012**, *965-968*.
11. Yang, Y.; Qiu, Z. B. Crystallization Kinetics and Morphology of Biodegradable Poly(butylene succinate-*co*-ethylene succinate) Copolyesters: Effects of Comonomer Composition and Crystallization Temperature. *CrystEngComm* **2011**, *13*, 2408-2417.
12. Li, X.; Qiu, Z. B. Crystallization Kinetics, Morphology, and Mechanical Properties of Novel Poly(ethylene succinate-*co*-octamethylene succinate). *Polym. Test.* **2015**, *48*, 125-132.
13. Xue, P.; Qiu, Z. B. Synthesis, Thermal Properties, and Crystallization Kinetics of Novel Biodegradable Poly(ethylene succinate-*co*-diethylene glycol succinate) Copolyesters. *Thermochim. Acta* **2015**, *606*, 45-52.
14. Papageorgiou, G. Z.; Bikiaris, D. N. Synthesis and Properties of Novel Biodegradable/Biocompatible Poly[propylene-*co*-(ethylene succinate)] Random Copolyesters. *Macromol. Chem. Phys.* **2009**, *210*, 1408-1421.
15. Zeng, J. B.; Zhu, Q. Y.; Lu, X.; He, Y.; Wang, Y. From Miscible to Partially Miscible Biodegradable Double Crystalline Poly(ethylene succinate)-*b*-poly(butylene succinate) Multiblock Copolyesters. *Polym. Chem.* **2012**, *3*, 399-408.
16. Wang, X. L.; Chen, S. C.; Zhang, Y. H. A Biodegradable Copolymer from Coupling Poly(*p*-dioxanone) with Poly(ethylene succinate) via Toluene-2, 4-diisocyanate. *E-Polymers.* **2009**, *9*:133-144.
17. Eiichi, Y.; Tomiya, I.; Tsuyoshi, S.; Yukio, Y. Process for the Production of Oxalic Acid. U.S. Pat., 3,678,107, 18 July 1972.
18. Garcia, J. J.; Miller, S. A. Polyoxalates from Biorenewable Diols



- via Oxalate Metathesis Polymerization. *Polym. Chem.* **2014**, *5*, 955-961.
19. Zhao, Y. H.; Xu, G. H.; Yuan, X. B. Novel Degradable Copolyesters Containing Poly(ethylene oxalate) Units Derived from Diethylene Oxalate. *Polym. Degrad. Stab.* **2006**, *91*, 101-107.
  20. Zuo, X. B.; Zhu Y. H.; Li, A. Y.; Ni, W.; Gao, P. Synthesis of Oxalic Acid Diethylene Glycol and Its Application in Polyester Polyols Preparation. *J. Chem. Eng. Chin. Univ.* **2011**, *25*, 799-802.
  21. Carothe, W. H.; Arvin, J. A.; Dorough, G. L. Studies on Polymerization and Formation Glycol Esters of Oxalic Acid. *J. Am. Chem. Soc.* **1930**, *52*, 3292-3300.
  22. Maeda, Y. Ring-opening Copolymerization of Succinic Anhydride with Ethylene Oxide Initiated by Magnesium Diethoxide. *Polymer* **1997**, *38*, 4719-4725.
  23. Avrami, M. Granulation, Phase Change, and Microstructure Kinetics of Phase Change. III. *J. Chem. Phys.* **1941**, *9*, 177-184.
  24. B. Wunderlich, *Macromolecular Physics*; vol. 2, Academic Press: New York, 1976.

**Publisher's Note** The Polymer Society of Korea remains neutral with regard to jurisdictional claims in published articles and institutional affiliations.